THE JOURNAL OF PHYSICAL CHEMISTRY A

Article

Cite This: J. Phys. Chem. A 2019, 123, 6304−6312

pubs.acs.org/JPCA

Interfaces of Gas−Aerosol Particles: Relative Humidity and Salt Concentration Effects

Published as part of The Journal of Physical Chemistry virtual special issue "Hai-Lung Dai Festschrift".

Yuqin Qian, Gang-hua Deng, Jordan Lapp, and Yi Rao*

Department of Chemistry and Biochemistry, Utah State University, Logan, Utah 84322, United States

ABSTRACT: The growth of aerosol particles is intimately related to chemical reactions in the gas phase and particle phase and at gas−aerosol particle interfaces. While chemical reactions in gas and particle phases are well documented, there is very little information regarding interface-related reactions. The interface of gas−aerosol particles not only facilitates a physical channel for organic species to enter and exit but also provides a necessary lane for culturing chemical reactions. The physical and chemical properties of gas−particle interfaces have not been studied extensively, nor have the reactions occurring at the interfaces been well researched. This is mainly due to the fact that there is a lack of suitable *in situ* interface-sensitive analytical techniques for direct measurements of interfacial properties. The motivation behind this research is to understand how interfaces play a role in the growth of aerosol particles. We have developed *in situ* interface-specific second harmonic scattering to examine interfacial behaviors of molecules of aerosol particles under different relative humidity (RH) and salt concentrations. Both the relative humidity and salt concentration can change the particle size and the phase of the aerosol. RH not only varies the concentration of solutes inside aerosol particles but also changes interfacial hydration in local regions. Organic molecules were found to exhibit distinct behaviors at the interfaces and bulk on NaCl particles under different RH levels. Our quantitative analyses showed that the interfacial adsorption free energies remain unchanged while interfacial areas increase as the relative humidity increases. Furthermore, the surface tension of NaCl particles decreases as the RH increases. Our experimental findings from the novel nonlinear optical scattering technique stress the importance of interfacial water behaviors on aerosol particles in the atmosphere.

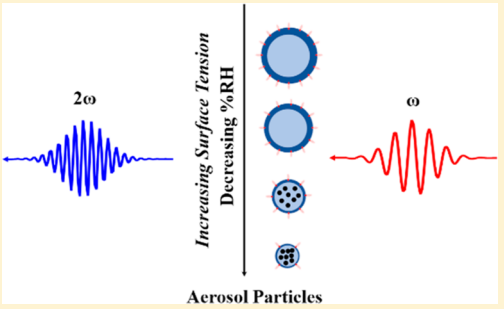

INTRODUCTION

Atmospheric aerosols are a colloidal system of tiny solid or liquid particles in the air. Such aerosol particles play an important role in atmospheric chemistry and climate uncertainty.[1,2] The growth of aerosol particles is closely related to chemical reactions in the gas phase and particle phase and at gas−aerosol particle interfaces.[1,3−10] All three phase reactions could become critical steps in the growth of aerosol particles, depending on relative humidity, temperature, and local environments (such as urban, forest, or marine conditions).[11−23] While chemical reactions occurring in gas and particle phases are well documented, interface-related information on aerosol particles is lacking.

Gas−particle interfaces are a localized region in which both organic and inorganic species are highly enriched. These species are expected to exhibit distinct physical and chemical properties from identical compounds in both gas and particle phases. Hydrophobic organic species preferentially adsorb onto gas−particle interfaces from particle phases. However, volatile organic compounds in the gas phase tend to be taken up into particle phases and partially remain on gas−particle interfaces. The gas−aerosol interfaces experience gas-phase diffusion, interfacial transport, and particle-phase diffusion in order to achieve gas−particle partitioning equilibrium. The interface of gas−aerosol particles not only facilitates a physical channel for organic species to enter and exit but also provides a necessary lane for culturing chemical reactions.[1,3,4,7,10,24−26] However, despite the significance of gas−aerosol interfaces, the physical and chemical properties of these gas−particle interfaces have not been studied extensively nor has there been significant research documenting interfacial chemical reactions and dynamics. This is mainly due to the fact that there is a lack of suitable *in situ* interface-sensitive analytical techniques for the direct measurements of interfacial properties.[1,27]

Second harmonic generation (SHG) and sum frequency generation (SFG) have been proven to be effective for investigations of liquid or solid planar surfaces.[28−41] Recently, Geiger and co-workers employed SFG to characterize surface species of atmospheric aerosol particles collected from different fields.[17,30,42] These early efforts demonstrated that SFG could probe interfacial structures of aerosol particles from different fields and locations; however, aerosol particles could experience loss of physical and chemical properties in the process of collection, transportation, and handling. Thus, probing interfaces of aerosols suspended in gases becomes imperative in real time, to some extent. However, second

Received: April 25, 2019
Revised: June 28, 2019
Published: June 28, 2019

DOI: 10.1021/acs.jpca.9b03896
J. Phys. Chem. A 2019, 123, 6304−6312

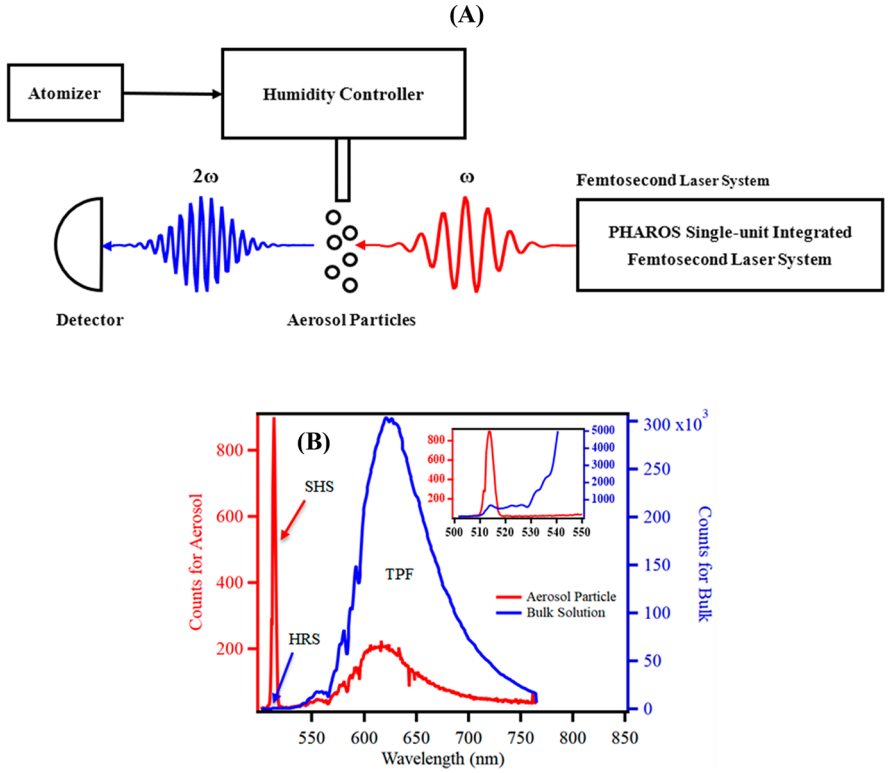

Figure 1. (A) Experimental setup for SHS measurement of the density of organic molecules (DIA-4) adsorbed to the aerosol surface and surface adsorption onto aerosol particles. The atomizer generates the aerosol particles. The humidity controller is used to change the humidity of aerosol particles. (B) Two-photon emission spectra from 500 to 765 nm for aerosol particles (red curve) and bulk solution (blue curve) from the same solution of 1.0 M NaCl in the presence of 7 μM DIA-4. The inset is the magnification of the curves.

harmonic scattering (SHS) and sum frequency scattering (SFS) have been developed for surfaces of micro- to nanometer size particles suspended in liquids.[28,43−50] We recently extended the SHS method into the *in situ* probe of the gas−aerosol particle interface.[51] This earlier report showed the first measurement of interfacial population of molecules from suspended aerosol particles with the particle density of 10^7 particles per cm^3 with a particle size around 100 nm. Recently, we have improved detection sensitivity to be 4 times as effective in detecting aerosol particles by implementing efficient detectors and effective light sources for nonlinear optical scattering.[52] Now our detection limit could reach a particle density of 10^3 particles per cm^3, which is comparable to real atmospheric settings. In this work, we further examine how relative humidity and salt concentration affect adsorption abilities of organic molecules at the gas−aerosol interface.

The motivation behind this research was to understand how interfaces play a role in the growth of sea aerosol particles as relative humidity and salt concentration are varied. Using NaCl particles to mimic sea aerosol, we can assess the role of these interfaces experimentally. Both the relative humidity and salt concentration can the change particle size and bulk phase of the aerosol. As far as relative humidity is concerned, its change is related to the deliquescent point, the size of aerosols internally mixed diameter, and particle optical properties from the gas−aerosol interface.[13,53−56] As relative humidity gradually increases around aerosol particles, solid salt particles absorb water and grow in size and weight. When RH is greater than the deliquescence point, these wet particles continue picking up more water to become a homogeneous solution particle. The salt concentration inside of aerosol particles could impact the surface tension of these particles. Surface tension of aerosol particles is assumed to be critical in activating to form cloud droplets, which unfortunately cannot be assessed experimentally with up-to-date methods. The particle size change could also affect the surface area of aerosol particles. A legitimate question arises about how water activity of aerosol particles influences the ability of facilitating molecules of the gas−aerosol interface. It is known that increasing the salt concentration in solution causes a salt-out effect, thereby decreasing the solubility of the solute in solution. Prior studies on how interfacial adsorption of organic molecules is affected by salt concentration were limited to air/water and oil/water interfaces,[16,33,57−68] without mention of the relative humidity effects of molecular adsorption at any interfaces. As we will show in this work, interfacial properties change as relative humidity varies.

EXPERIMENTAL SECTION

Second Harmonic Generation (SHG) Measurement. A schematic of the experimental setup for our second harmonic measurements is shown in Figure 1A. The experimental setup includes three components, *the laser source, particle generation and handling, and signal collection and detection*, as referenced in our previous work.[51,52]

1. Laser Source. A 10 W femtosecond laser system (PHAROS, Light Conversion) was used in our experiments. The femtosecond laser was centered at a fixed wavelength of 1030 nm, with a tunable repetition rate from a single shot to 1 MHz (290 fs). A 1 MHz repetition rate was used in our experiments alongside a lens of a focal length of 10 cm, directed to focus onto a flow of aerosol particles.

DOI: 10.1021/acs.jpca.9b03896
J. Phys. Chem. A 2019, 123, 6304−6312

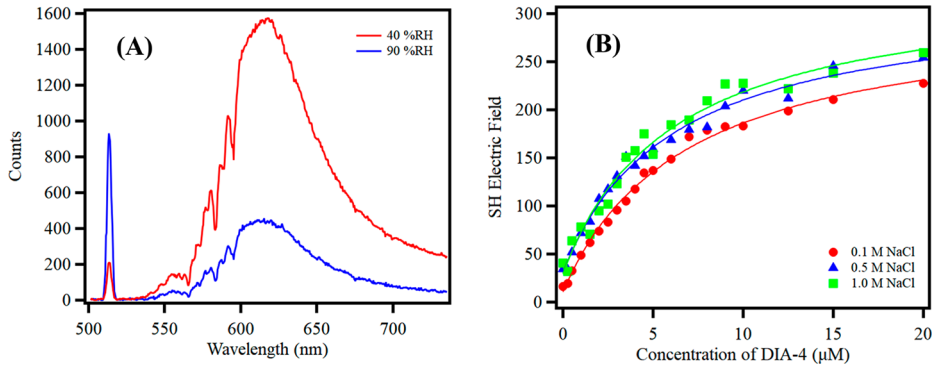

Figure 2. (A) Coherent SHS spectra from the gas−aerosol particle interfaces under two different RHs of 40% and 90%. The aerosol particles were generated by a same solution of 1.0 M NaCl with 20 μM DIA-4. The two-photon emission spectra show that the aerosol particles at 40% RH have the lower SHS signal on the gas−aerosol particle interface and the larger TPF signals from particle phase than those at 90% RH. (B) SHS isotherms of aerosol particles for different NaCl concentrations solutions of 0.1, 0.5, and 1.0 M with increasing DIA-4 concentration.

2. Particle Generation and Handling. A solution of NaCl acted as a seed solution for the generation of aerosol particles in our experiments. Aerosol particles were generated by compressing nitrogen gas at a pressure of 40 psi with a constant output atomizer (TSI 3076). The seed solution was drawn by the nitrogen gas with a controlled rate of 4 L/min. An optical particle sizer (TSI 3330, detection size of >300 nm) together with a nanoparticle sizer (TSI 3910, detection size of 10−300 nm) was used to measure size distribution of the laboratory-generated aerosol particles. The aerosol particles were diluted 100 times by an aerosol diluter (TSI 3332) before the sizers. The size of the aerosol particles is mainly centered at ca. 60 nm with a broad distribution of ca. 120 nm (full width at half-maximum). The total number density distribution was estimated to be ca. 2.1×10^6 particles per cm^3 from the number distribution. A well-sealed chamber with a footprint area of 40 cm × 30 cm and a height of 30 cm was built to prevent aerosol particle leakage. In addition, a pump with a controllable rate was used to exhaust aerosol particles after experiments in order to avoid accumulation of particles in the chamber.

3. Signal Collection and Detection. A lens of 2 in. diameter aperture with 2 cm focal length was used in a forward geometry to collect SHS signals directly into a spectrometer. As such, an SHS signal of a scattering angle of almost 60 degrees was collected in our SHS measurements. A spectrometer (Acton 300i, Princeton Instruments) equipped with a charge coupled device (Princeton Instruments, LN/CCD-1340/400) constituted the SHS detection system. A WinSpec program from Princeton Instruments was used to record spectra from the CCD. Two short-pass filters with a cutoff wavelength of 900 nm and the spectrometer separated SHS photons from the fundamental 1030 nm beam and any background signal.

To control the relative humidity of aerosol particles, a home-built humidity controller was made. Aerosol particles were generated by dry nitrogen gas with 4 L/min flow rate. Relative humidity for as-prepared aerosols was higher than 90% RH. The as-prepared aerosol particles were passed through silica gel drier (290 mm long, 64 mm inner diameter) to keep aerosol particles less than 30% relative humidity. After that, RH for aerosol particles was increased by a humidifier, which was composed of permeable Teflon tubing (Zeus, Inc.) with a 6 mm o.d., which was located inside a copper tube of a 13 mm o.d. and 200 mm length. The gap between the copper tube and the Teflon tube was filled with ultrapure water. The copper tube was covered with heating tape to control the external temperature in order to be kept at the desired stationary temperatures for each different relative humidity using a feedback looped temperature controller and a thermocouple. The relative humidity was monitored by a humidity transmitter (HX200 series, OMEGA Engineering, Inc.).

Chemicals. To investigate interfacial responses of aerosol particles, we used a SHG-active dye as an indicator. The choice of dye has to be interface-active, meaning that the dye has to be populated at the gas−aerosol interface. *trans*-4-[4-(Dibutylamino)styryl]-1-methylpyridinium iodide (DIA-4) was chosen to meet the requirements. DIA-4 was purchased from Sigma-Aldrich as received. Ultrapure water of 18.2 MΩ·cm was used in our experiments. NaCl (Fisher Chemical) was baked at 600 °C for 10 h prior to use.

RESULTS AND DISCUSSION

SHS from gas−aerosol particle interfaces radiates coherently due to a fixed phase relationship from dipoles located on the particles,[44] whereas hyperRayleigh scattering (HRS) from bulk diploes contributes to incoherent second-order responses originating from instantaneous noncentrosymmetric breaking of density fluctuations. Both the coherent SHS and incoherent HRS are two-photon processes, of which energy is in the same region of a double frequency (2ω) for experimental measurements for a given fundamental light frequency (ω). Even though the coherent SHS responses are proportional to the second power of interfacial dipole densities and the incoherent HRS signal is simply proportional to bulk dipole densities, it is hard to differentiate one from the other. In an effort to prove if two-photon emission at the 2ω comes from coherent SHS, we used two-photon fluorescence (TPF) as a reference.[51,52] Since both TPF and HRS are two-photon bulk processes, their signals are proportional to the solution concentration. The ratio of HRS to TPF for a given sample remains the same if only bulk contributes to two-photon emissions. Thus, the ratio of signal at a double frequency (2ω) to TPF will be used as a benchmark to justify if the signal at 2ω comes from bulk or interfaces.

To verify if the gas−aerosol interface generates the SHS signal, two-photon emission experiments for aerosol particles were carried out under 1030 nm photoexcitation. Control experiments were also performed for solution under the same experimental conditions. Both the aerosol particle and solution

DOI: 10.1021/acs.jpca.9b03896
J. Phys. Chem. A 2019, 123, 6304−6312

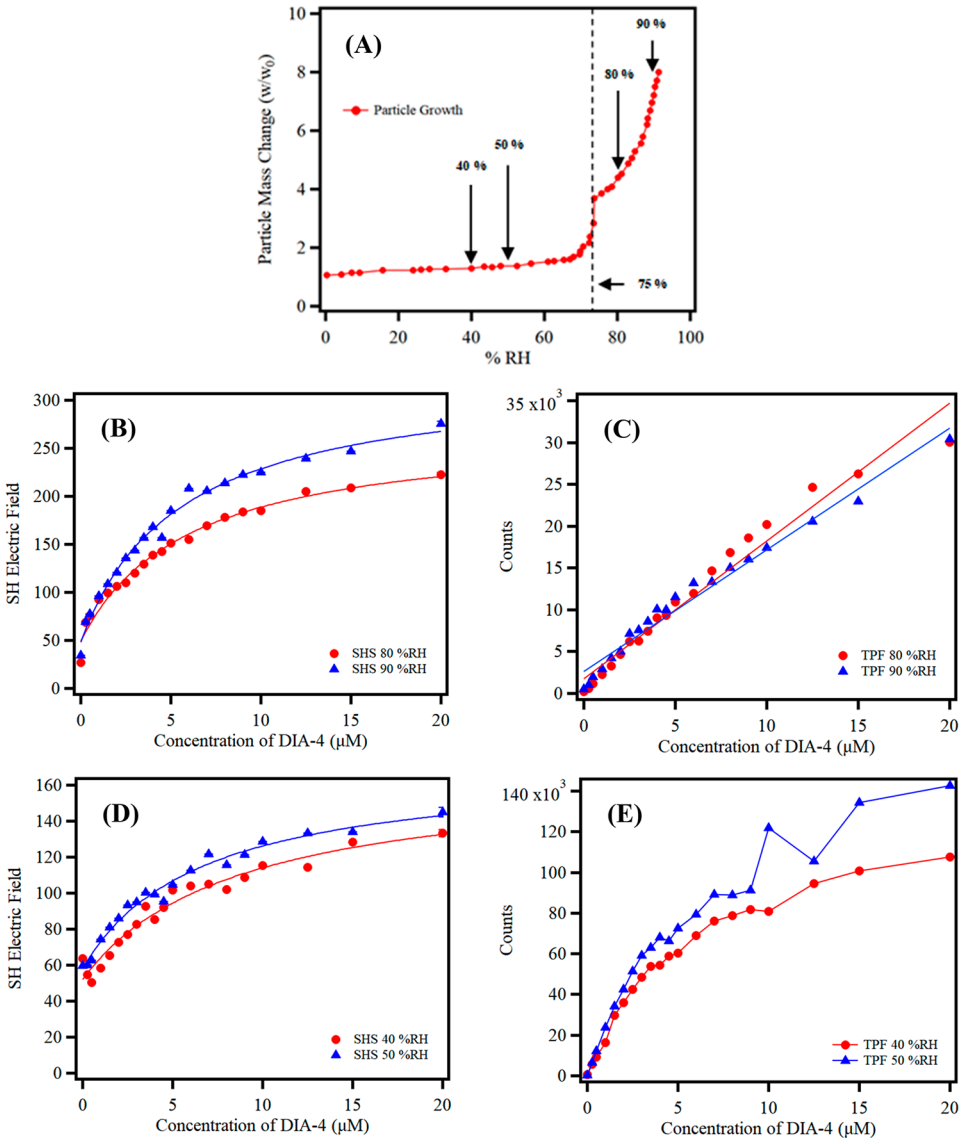

Figure 3. (A) Hygroscopic growth of pure NaCl particles as a function of relative humidity.[54] The NaCl particles increase in mass very slowly up until 75% RH. Above that point, the NaCl particles grow continuously with increasing RH. (B), (C) SHS at 515 nm and TPF at 620 nm as a function of DIA-4 concentration in 1.0 M NaCl solution for the aerosol particles at higher RHs of 80% and 90%, respectively. (D), (E) SHS at 515 nm and TPF at 620 nm as a function of DIA-4 concentration in 1.0 M NaCl solution for the aerosol particles at the lower RHs of 40% and 50%, respectively.

were from the same stock solution of 1.0 M NaCl in the presence of 7 μM DIA-4. Figure 1B presents the two-photon emission spectra from 500 to 765 nm for aerosol particles (red curve) and the solution (blue curve). Both curves exhibit a broad peak centered at 620 nm, which can be attributed to two-photon florescence of DIA-4. To assign the sharp peaks signal at 515 nm for the aerosol particles and solution, we compared their ratios with respect to TPF. The signal at 515 nm for the solution of DIA-4 is much smaller than the TPF signal at 620 nm, which has an intensity ratio of 2.28×10^{-3}. However, the signal for the aerosol particles at 515 nm is much larger than the TPF signal at 620 nm, which has an intensity ratio of 4.40. The large signal at 515 nm from the aerosol particles could not be from their particle phase since the amount of DIA-4 in the particle phase is much less than that in the solution. Therefore, the signal at 515 nm from the aerosol particles must be attributed to coherent SHS from the gas–aerosol particle interface.

Knowing that DIA-4 molecules are populated at the gas–aerosol particle interface, we now must investigate how relative humidity affects interfacial behaviors of the aerosol particles. Two-photon emission experiments for DIA-4 from aerosol particles were carried out under two different RHs of 40% and 90%. Figure 2A shows that two-photon emission spectra are distinct under the two RHs for aerosol particles generated from 1.0 M NaCl with 20 μM DIA-4. In the case of interfacial responses of aerosol particles, the SHS signal at 40% RH was found to be lower than that at 90% RH. However, the TPF signal is larger at 40% RH than at 90% RH in the particle phase. These results suggest that interfacial behaviors and bulk responses are significantly different for dry and wet aerosol particles as RH changes.

To understand how salt concentration affects adsorption ability of organic molecules at the gas–aerosol interface, SHS experiments were carried out for aerosols generated from different concentrations of NaCl solutions. The coherent SHSs

DOI: 10.1021/acs.jpca.9b03896
J. Phys. Chem. A 2019, 123, 6304–6312

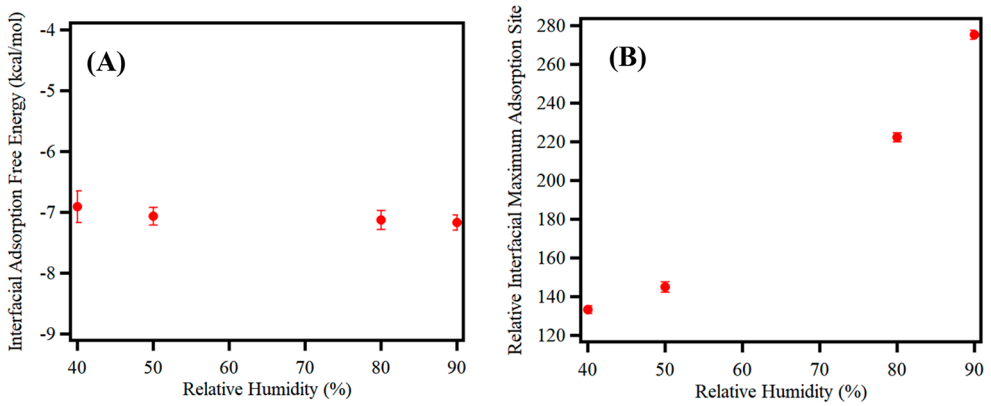

Figure 4. (A) Interfacial adsorption free energy (ΔG) of DIA-4 at the gas−aerosol particle interface obtained from the SHS isotherms from Figure 3 as a function of RH for NaCl aerosol particles. (B) Relative interfacial maximum adsorption site N_R as a function of RH.

of aerosol particles were taken as a function of concentrations, so-called SHS isotherms. Figure 2B compares three SHG isotherms of DIA-4 for aerosols by three different concentrations NaCl solutions, including 0.1, 0.5, and 1.0 M, at the relative humidity of 85%. The three SHS isotherms are nearly identical. These aerosols have a similar interfacial binding constant, independent of salt concentrations in particle phase.

It is known that NaCl aerosol particles undergo phase transitions under different relative humidity.[54] A deliquescent point for NaCl particles occurs at a RH of 75%.[54] Above the deliquescent point, only the liquid phase occurs in NaCl aerosol particles. As the RH decreases, aerosol particles lose their mass by water evaporation. Below the deliquescent point, both solid and liquid phases coexist in NaCl aerosol particles. Hygroscopic growth of pure NaCl particles as a function of relative humidity is sketched in Figure 3A. To further investigate how water vapor affects interfacial molecular population of aerosols, we chose two regions, one below the deliquescence point and the other above the deliquescence point. In the region below the deliquescence point, two RHs of 40% and 50% were examined. In the case above the deliquescence point, two RHs of 80% and 90% were tested. The intensity ratios between SHS and TPF are 1.35 at 80% RH, and 2.07 at 90% RH. The SHS isotherm measurements were carried out under the four different RHs of DIA-4 at the gas−aerosol interface. Parts B and C of Figure 3 compare the SHS at 515 nm and TPF at 620 nm as a function of DIA-4 concentration in 1.0 M NaCl solution for the aerosol particles at the higher RHs of 80% and 90%. The SHS isotherms show typical adsorption behaviors at interfaces above the deliquescent point. In this region, TPF intensities exhibit a linear relation with increasing concentration as expected. Parts D and E of Figure 3 compare the SHS at 515 nm and TPF at 620 nm as a function of the DIA-4 concentration in 1.0 M NaCl solution for the aerosol particles below the deliquescent point. Below the deliquescent point, the SHS isotherms show typical adsorption behaviors at interfaces with RHs of 40% and 50%. The intensity ratios between SHS and TPF are 0.13 at 40% RH, and 0.12 at 50% RH. Interestingly, TPF intensities were found to vary nonlinearly with increasing concentrations of DIA-4, showcasing DIA-4's sensitivity to changes in environment.[69−71] These nonlinear responses might arise from saturation of DIA-4 in NaCl particles when water contents get smaller. Relative humidity affects actual vapor pressure around aerosol particles. Thermodynamically, RH determines the concentration of salt in aerosols. A lower RH below the deliquescence point leads to a higher salt concentration of aerosols.[13,53,54] Moreover, relative humidity could impact interfacial water activities of aerosols from our SHS measurements, thereby modulating the interfacial population of organic molecules on the particles. Our results suggest that RH not only varies the concentration of solutes inside aerosol particles but also changes interfacial hydration in local regions.

To quantitatively reveal adsorption of organic molecules at the gas−aerosol particle interface, we start to introduce a basic principle of coherent SHS. Coherent SHS intensity (I_{SHS}) is related to interfacial electric field, E_{SHS}, which is given by[29,33,72]

$$I_{SHS} \propto |E_{SHS}|^2 \tag{1}$$

Interfacial electric field is proportional to interfacial density N_s. Assuming that interfacial population follows a Langmuir model, the interfacial electric field is expresses as follows,[43,60,67,68,72−74]

$$E_{SHS} \propto N_s \propto \frac{KcN_\infty}{Kc + 1} \tag{2}$$

where K represents the equilibrium constant of the interfacial adsorption, c the concentration of DIA-4 in solution, and N_∞ interfacial maximum adsorption site. For an estimated surface area of 40 Å^2 per DIA-4 molecule, a single aerosol particle of 100 nm could host a maximum number of ca. 1.57×10^4 DIA-4 molecules for one monolayer at the interface. Recent studies show that concentration of a molecule could exceed several times its saturation concentration.[75] Even so, the DIA-4 molecules are highly enriched at the gas−aerosol particle interfaces.

In an effort to examine interfacial adsorption behaviors under the four different RHs, we attempted to extract interfacial adsorption equilibrium constants for them with eq 2. The K values for the interfacial adsorption constants under the RHs of 80% and 90% below the deliquescent point of NaCl particles were found to be similar, which are 9.32 ± 1.45 and 10.08 ± 1.22 μM^{-1}, respectively. Above the deliquescent point, the values for the interfacial adsorption constants under the RHs of 40% and 50% are 6.46 ± 1.65 and 8.40 ± 1.26 μM^{-1}, respectively. The interfacial adsorption free energies for the four RHs were calculated, according to $\Delta G = -RT \ln K/55.5$.[60,72] Figure 4A presents the interfacial adsorption free energies for the four RHs from our experiments. The values of ΔG remain almost constant with increasing RHs, suggesting that the interfacial driving forces for an aerosol particle are

DOI: 10.1021/acs.jpca.9b03896
J. Phys. Chem. A 2019, 123, 6304−6312

similar under different RHs. In eq 2, we mentioned the interfacial maximum adsorption site N_∞ but could not obtain it directly. However, we could calculate relative interfacial maximum adsorption site N_R as a function of RH shown in Figure 4B, The N_R is defined as follows:

$$N_R = \frac{N_s}{N_\infty} \tag{3}$$

The N_R becomes larger as the RH increases. From 40% to 90% RH, the accessible adsorption sites increase by a factor of 2. This change in the N_R is intimately related to the increase in the area of aerosol particles with increasing RH. Our SHS results directly provide information about both the interfacial driving force and size of aerosol particles.

While it is too early to correlate our experimental results with the atmospheric activity of cloud condensation nucleus (CCN), it is still necessary to tentatively explain how interfacial information obtained from our laboratory is related to atmospheric events. CCN activity is a complex function of aerosol size, shape, and chemical composition and is an important metric for investigating aerosol impacts on climate and the environment. Activation is necessary to form a cloud droplet from an aerosol particle and is assumed to occur as soon as a wetted particle grows beyond its critical radius. The activation of aerosol particles into cloud droplets requires surface tension of atmospheric particles in addition to the Raoult's term describing the surrounding water vapor. However, there is no method or instrument capable of measuring these parameters of aerosol particles, namely, surface tension of aerosol particles. The Köhler theory connects the equilibrium size of a hygroscopically grown solution particle with the water vapor saturation at its interface (S_d)[53,76]

$$S_d = Q_K a_w \tag{4}$$

where Q_K is the Kelvin term and a_w is the Raoult term related to water activity. The Raoult term remains almost constant in our case since DIA-4 has low vapor pressure. Here we focus only on the Kelvin term. A particle of liquid in its own vapor will result in a convex liquid interface with the vapor. The Kelvin term depends critically on the surface tension of the particle σ_s. The size of the particle d_d in the Kelvin term accounts for the curvature of the particles. It is, furthermore, composed of the molecular weight of water M_w, the ideal gas constant R, the temperature T, and the density of water ρ_w.[44,65]

$$Q_K = \exp\left(\frac{4M_w\sigma_s}{RT\rho_w d_d}\right) \tag{5}$$

According to a university standard edition physical chemistry textbook,[77,78] surface tension is given by

$$\sigma_s = \left(\frac{\partial G}{\partial A_w}\right)_{T,P} \tag{6}$$

where G is free energy and A_w is the molar surface area of particle for given temperature (T) and pressure (P). From our measurements, ΔG values remain unchanged and the areas A_w increase with varying RH. The σ_s qualitatively decreases with increasing RH. Aerosol particles of higher RH have larger growth factor and thereby decrease surface tension. Hydrophobic molecules should prefer to activate into cloud droplets with a decrease in surface tension of atmospheric particles.

The surface tension of an aqueous solution σ_s can be further approximated as[74]

$$\sigma_s = \sigma_w + \frac{RT}{A_w}\ln\frac{a_w^s}{a_w^b} \tag{7}$$

where σ_w is the surface tension of pure water, A_w is the molar surface area of the particle, a_w^s is the water activity in the surface, and a_w^b is the water activity in the bulk. The surface tension of aerosol particles decreases, suggesting that a_w^s is less than a_w^b. In other words, interfacial water activity is smaller than bulk water activity; however, there is no explicit expression for interfacial water activity reported in the literature. Interfacial water exists in a few layers to the nanometer region on aerosol particles. Macroscopically, interfacial water activity reflects the ability for facilitating alien molecules, which is related to surface tension. Interfacial water has significant effects on surface tension and accommodation ability of both organic and inorganic species. The degree of hydration and the number of water molecules in the first hydration shell of the interfacial solute molecules of the gas−aerosol particle are expected to be different from those at the planar gas/water interface.

The Extended Aerosol Inorganic Model (E-AIM) is often used to calculate surface tension under different relative humidities of aerosol particles.[26] The chemical system for this model consists of a gas phase, inorganic and organic solids phase, and two liquid phases. One of the liquid phases is aqueous and the other phase is hydrophobic. The aqueous phase can contain both inorganic electrolytes and dissolved organic compounds, whereas the hydrophobic phase can contain only organic compounds. The surface tension of the aqueous phase, including organic solutes, could be calculated using the model of Dutcher et al.[79] However, this model assumes that all solutes have to be fully mixed within the aqueous phase. Therefore, the E-AIM model is not suitable for "surface active" compounds that concentrate at the gas−aerosol particle interface, such as DIA-4 molecules in our work.

Taken together, we proposed a schematic of interfacial behaviors of molecules for aerosol particles in Figure 5. This schematic displays interfacial population of organic species onto aerosol particles of different salt concentration with varying RH. For a given RH, interfacial adsorption ability of organic species remains almost the same as concentrations of sodium chloride solution change. Furthermore, interfacial adsorption ability of organic species remains constant as the

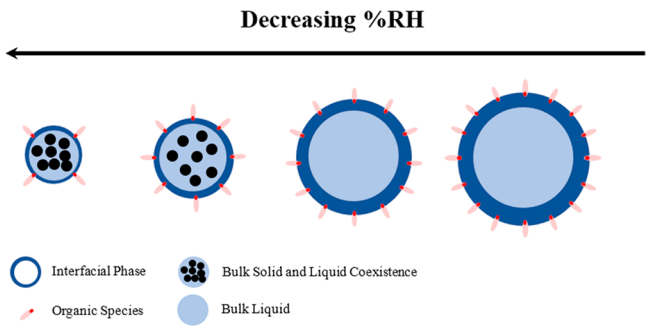

Figure 5. Schematic of interfacial behaviors of organic species on aerosols of different NaCl concentrations with varying RH. Surface tension of aerosol particles decreases with increasing RHs. The interfacial adsorption ability remains almost the same as NaCl concentrations increase.

DOI: 10.1021/acs.jpca.9b03896
J. Phys. Chem. A 2019, 123, 6304−6312

RH varies as well. The surface tension decreases as the RH increases, which accompanies an increase in size for aerosol particles.

SUMMARY AND CONCLUSIONS

We have demonstrated *in situ* detection of organic species at gas−aerosol particle interfaces by developing second harmonic scattering technique. This novel nonlinear optical scattering method has enabled us to reveal interfacial behaviors of organic species of aerosol particles in real time. Interfacial population of organic species have been examined under different concentrations of NaCl and different relative humidity. It has been found that organic species, DIA-4 molecules, exhibit distinct behaviors at the interfaces and bulk on NaCl particles under different relative humidity. Our quantitative analyses have shown that the interfacial adsorption free energies remain unchanged and interfacial areas increase as relative humidity increase, and surface tension of NaCl particles decreases as RH increases. Our experimental findings from the novel technique stress the importance of interfacial water activity on aerosol particles. We believe that these preliminary results could deepen the understanding of activation of cloud condensation activities in the atmosphere and will be important to account for when modeling the activation of aerosol particles to cloud droplets.

AUTHOR INFORMATION

Corresponding Author

*Yi Rao. Phone: 435-797-0640. E-mail: yi.rao@usu.edu.

ORCID

Yi Rao: 0000-0001-9882-1314

Notes

The authors declare no competing financial interest.

ACKNOWLEDGMENTS

Y.R acknowledges financial support from the National Science Foundation grant CHE-1506789. The authors are thankful for Dr. V. Faye McNeill for her help in the control of relative humidity.

REFERENCES

(1) Finlayson-Pitts, B. J. Reactions at Surfaces in the Atmosphere: Integration of Experiments and Theory as Necessary (but Not Necessarily Sufficient) for Predicting the Physical Chemistry of Aerosols. *Phys. Chem. Chem. Phys.* **2009**, *11*, 7760−79.

(2) Seinfeld, J. H.; Pandis, S. N. *Atmospheric Chemistry and Physics: From Air Pollution to Climate Change*, 2nd ed.; Wiley: Hoboken, NJ, 2006; p 1232.

(3) Virtanen, A.; Joutsensaari, J.; Koop, T.; Kannosto, J.; Yli-Pirila, P.; Leskinen, J.; Makela, J. M.; Holopainen, J. K.; Poschl, U.; Kulmala, M.; et al. An Amorphous Solid State of Biogenic Secondary Organic Aerosol Particles. *Nature* **2010**, *467*, 824−7.

(4) McNeill, V. F. Aqueous Organic Chemistry in the Atmosphere: Sources and Chemical Processing of Organic Aerosols. *Environ. Sci. Technol.* **2015**, *49*, 1237−44.

(5) Wingen, L. M.; Moskun, A. C.; Johnson, S. N.; Thomas, J. L.; Roeselova, M.; Tobias, D. J.; Kleinman, M. T.; Finlayson-Pitts, B. J. Enhanced Surface Photochemistry in Chloride-Nitrate Ion Mixtures. *Phys. Chem. Chem. Phys.* **2008**, *10*, 5668−77.

(6) Reid, J. P.; Sayer, R. M. Heterogeneous Atmospheric Aerosol Chemistry: Laboratory Studies of Chemistry on Water Droplets. *Chem. Soc. Rev.* **2003**, *32*, 70−9.

(7) Li, W. Y.; Li, X.; Jockusch, S.; Wang, H.; Xu, B.; Wu, Y.; Tsui, W. G.; Dai, H. L.; McNeill, V. F.; Rao, Y. Photoactivated Production of Secondary Organic Species from Isoprene in Aqueous Systems. *J. Phys. Chem. A* **2016**, *120*, 9042−9048.

(8) Fu, H.; Ciuraru, R.; Dupart, Y.; Passananti, M.; Tinel, L.; Rossignol, S.; Perrier, S.; Donaldson, D. J.; Chen, J.; George, C. Photosensitized Production of Atmospherically Reactive Organic Compounds at the Air/Aqueous Interface. *J. Am. Chem. Soc.* **2015**, *137*, 8348−51.

(9) Smith, J. D.; Sio, V.; Yu, L.; Zhang, Q.; Anastasio, C. Secondary Organic Aerosol Production from Aqueous Reactions of Atmospheric Phenols with an Organic Triplet Excited State. *Environ. Sci. Technol.* **2014**, *48*, 1049−57.

(10) Tsui, W. G.; Rao, Y.; Dai, H. L.; McNeill, V. F. Modeling Photosensitized Secondary Organic Aerosol Formation in Laboratory and Ambient Aerosols. *Environ. Sci. Technol.* **2017**, *51*, 7496−7501.

(11) Fan, H.; Tinsley, M. R.; Goulay, F. Effect of Relative Humidity on the OH-Initiated Heterogeneous Oxidation of Monosaccharide Nanoparticles. *J. Phys. Chem. A* **2015**, *119*, 11182−11190.

(12) Tang, M.; Larish, W. A.; Fang, Y.; Gankanda, A.; Grassian, V. H. Heterogeneous Reactions of Acetic Acid with Oxide Surfaces: Effects of Mineralogy and Relative Humidity. *J. Phys. Chem. A* **2016**, *120*, 5609−5616.

(13) Mauer, L. J.; Taylor, L. S. Water-Solids Interactions: Deliquescence. *Annu. Rev. Food Sci. Technol.* **2010**, *1*, 41−63.

(14) Muscatello, J.; Chacón, E.; Tarazona, P.; Bresme, F. Deconstructing Temperature Gradients across Fluid Interfaces: The Structural Origin of the Thermal Resistance of Liquid-Vapor Interfaces. *Phys. Rev. Lett.* **2017**, *119*. DOI: 10.1103/PhysRevLett.119.045901

(15) Cui, Z.-X.; Zhao, M.-Z.; Lai, W.-P.; Xue, Y.-Q. Thermodynamics of Size Effect on Phase Transition Temperatures of Dispersed Phases. *J. Phys. Chem. C* **2011**, *115*, 22796−22803.

(16) Hensel, J. K.; Carpenter, A. P.; Ciszewski, R. K.; Schabes, B. K.; Kittredge, C. T.; Moore, F. G.; Richmond, G. L. Molecular Characterization of Water and Surfactant AOT at Nanoemulsion Surfaces. *Proc. Natl. Acad. Sci. U. S. A.* **2017**, *114*, 13351−13356.

(17) Ebben, C. J.; Shrestha, M.; Martinez, I. S.; Corrigan, A. L.; Frossard, A. A.; Song, W. W.; Worton, D. R.; Petaja, T.; Williams, J.; Russell, L. M.; et al. Organic Constituents on the Surfaces of Aerosol Particles from Southern Finland, Amazonia, and California Studied by Vibrational Sum Frequency Generation. *J. Phys. Chem. A* **2012**, *116*, 8271−90.

(18) Kahan, T. F.; Wren, S. N.; Donaldson, D. J. A Pinch of Salt is All It Takes: Chemistry at the Frozen Water Surface. *Acc. Chem. Res.* **2014**, *47*, 1587−94.

(19) You, Y.; Renbaum-Wolff, L.; Carreras-Sospedra, M.; Hanna, S. J.; Hiranuma, N.; Kamal, S.; Smith, M. L.; Zhang, X.; Weber, R. J.; Shilling, J. E.; et al. Images Reveal that Atmospheric Particles can Undergo Liquid-Liquid Phase Separations. *Proc. Natl. Acad. Sci. U. S. A.* **2012**, *109*, 13188−93.

(20) Anim-Danso, E.; Zhang, Y.; Alizadeh, A.; Dhinojwala, A. Freezing of Water Next to Solid Surfaces Probed by Infrared-Visible Sum Frequency Generation Spectroscopy. *J. Am. Chem. Soc.* **2013**, *135*, 2734−40.

(21) Buch, V.; Groenzin, H.; Li, I.; Shultz, M. J.; Tosatti, E. Proton Order in the Ice Crystal Surface. *Proc. Natl. Acad. Sci. U. S. A.* **2008**, *105*, 5969−74.

(22) Krepelova, A.; Huthwelker, T.; Bluhm, H.; Ammann, M. Surface Chemical Properties of Eutectic and Frozen NaCl Solutions Probed by XPS and NEXAFS. *ChemPhysChem* **2010**, *11*, 3859−66.

(23) Lovering, K. A.; Bertram, A. K.; Chou, K. C. Transient Phase of Ice Observed by Sum Frequency Generation at the Water/Mineral Interface During Freezing. *J. Phys. Chem. Lett.* **2017**, *8*, 871−875.

(24) Das, P. K. Chemical Applications of Hyper-Rayleigh Scattering in Solution. *J. Phys. Chem. B* **2006**, *110*, 7621−30.

(25) Jimenez, J. L.; Canagaratna, M. R.; Donahue, N. M.; Prevot, A. S.; Zhang, Q.; Kroll, J. H.; DeCarlo, P. F.; Allan, J. D.; Coe, H.; Ng, N. L.; et al. Evolution of Organic Aerosols in the Atmosphere. *Science* **2009**, *326*, 1525−9.

DOI: 10.1021/acs.jpca.9b03896
J. Phys. Chem. A 2019, 123, 6304−6312

(26) Rothfuss, N. E.; Petters, M. D. Influence of Functional Groups on the Viscosity of Organic Aerosol. *Environ. Sci. Technol.* **2017**, *51*, 271−279.
(27) Kolb, C. E.; Worsnop, D. R. Chemistry and Composition of Atmospheric Aerosol Particles. *Annu. Rev. Phys. Chem.* **2012**, *63*, 471−491.
(28) Roke, S.; Roeterdink, W. G.; Wijnhoven, J. E.; Petukhov, A. V.; Kleyn, A. W.; Bonn, M. Vibrational Sum Frequency Scattering from a Submicron Suspension. *Phys. Rev. Lett.* **2003**, *91*, 258302.
(29) Shen, Y. R. Surface Properties Probed by Second Harmonic and Sum Frequency Generation. *Nature* **1989**, *337*, 519−525.
(30) Geiger, F. M. Second Harmonic Generation, Sum Frequency Generation, and $X^{(3)}$: Dissecting Environmental Interfaces with a Nonlinear Optical Swiss Army Knife. *Annu. Rev. Phys. Chem.* **2009**, *60*, 61−83.
(31) Wang, H.-F.; Gan, W.; Lu, R.; Rao, Y.; Wu, B.-H. Quantitative Spectral and Orientational Analysis in Surface Sum Frequency Generation Vibrational Spectroscopy (SFG-VS). *Int. Rev. Phys. Chem.* **2005**, *24*, 191−256.
(32) Rao, Y.; Li, X.; Lei, X.; Jockusch, S.; George, M. W.; Turro, N. J.; Eisenthal, K. B. Observations of Interfacial Population and Organization of Surfactants with Sum Frequency Generation and Surface Tension. *J. Phys. Chem. C* **2011**, *115*, 12064−12067.
(33) Richmond, G. L. Molecular Bonding and Interactions at Aqueous Surfaces as Probed by Vibrational Sum Frequency Spectroscopy. *Chem. Rev.* **2002**, *102*, 2693−2724.
(34) Jubb, A. M.; Hua, W.; Allen, H. C. Environmental Chemistry at Vapor/Water Interfaces: Insights from Vibrational Sum Frequency Generation Spectroscopy. *Annu. Rev. Phys. Chem.* **2012**, *63*, 107−130.
(35) Yan, E. C. Y.; Eisenthal, K. B. Probing the Interface of Microscopic Clay Particles in Aqueous Solution by Second Harmonic Generation. *J. Phys. Chem. B* **1999**, *103*, 6056−6060.
(36) Xiong, W.; Laaser, J. E.; Mehlenbacher, R. D.; Zanni, M. T. Adding a Dimension to the Infrared Spectra of Interfaces Using Heterodyne Detected 2D Sum-Frequency Generation (HD 2D SFG) Spectroscopy. *Proc. Natl. Acad. Sci. U. S. A.* **2011**, *108*, 20902−7.
(37) Fourkas, J. T.; Walker, R. A.; Can, S. Z.; Gershgoren, E. Effects of Reorientation in Vibrational Sum-Frequency Spectroscopy†. *J. Phys. Chem. C* **2007**, *111*, 8902−8915.
(38) Chen, Z.; Shen, Y. R.; Somorjai, G. A. Studies of Polymer Surfaces by Sum Frequency Generation Vibrational Spectroscopy. *Annu. Rev. Phys. Chem.* **2002**, *53*, 437−465.
(39) Ma, Y.; Hou, J.; Hao, W.; Liu, J.; Meng, L.; Lu, Z. Influence of Riboflavin on the Oxidation Kinetics of Unsaturated Fatty Acids at the Air/Aqueous Interface Revealed by Sum Frequency Generation Vibrational Spectroscopy. *Phys. Chem. Chem. Phys.* **2018**, *20*, 17199−17207.
(40) Kim, G.; Gurau, M.; Kim, J.; Cremer, P. S. Investigations of Lysozyme Adsorption at the Air/Water and Quartz/Water Interfaces by Vibrational Sum Frequency Spectroscopy. *Langmuir* **2002**, *18*, 2807−2811.
(41) Dhar, P.; Plymale, N. T.; Malyk, S.; Lewis, N. S.; Benderskii, A. V. Vibrational Sum-Frequency Spectroscopic Investigation of the Structure and Azimuthal Anisotropy of Propynyl-Terminated Si(111) Surfaces. *J. Phys. Chem. C* **2017**, *121*, 16872−16878.
(42) Shrestha, M.; Zhang, Y.; Ebben, C. J.; Martin, S. T.; Geiger, F. M. Vibrational Sum Frequency Generation Spectroscopy of Secondary Organic Material Produced by Condensational Growth from Alpha-Pinene Ozonolysis. *J. Phys. Chem. A* **2013**, *117*, 8427−36.
(43) Wang, H.; Yan, E. C. Y.; Borguet, E.; Eisenthal, K. B. Second Harmonic Generation from the Surface of Centrosymmetric Particles in Bulk Solution. *Chem. Phys. Lett.* **1996**, *259*, 15−20.
(44) Dadap, J. I.; Shan, J.; Heinz, T. F. Theory of Optical Second-Harmonic Generation from a Sphere of Centrosymmetric Material: Small-Particle Limit. *J. Opt. Soc. Am. B* **2004**, *21*, 1328−1347.
(45) Gan, W.; Gonella, G.; Zhang, M.; Dai, H. L. Communication: Reactions and Adsorption at the Surface of Silver Nanoparticles Probed by Second Harmonic Generation. *J. Chem. Phys.* **2011**, *134*, 041104.
(46) Roke, S.; Bonn, M.; Petukhov, A. V. Nonlinear Optical Scattering: The Concept of Effective Susceptibility. *Phys. Rev. B: Condens. Matter Mater. Phys.* **2004**, *70*, 115106.
(47) Roke, S.; Gonella, G. Nonlinear Light Scattering and Spectroscopy of Particles and Droplets in Liquids. *Annu. Rev. Phys. Chem.* **2012**, *63*, 353−378.
(48) Wang, H.-F.; Troxler, T.; Yeh, A.-G.; Dai, H.-L. Adsorption at a Carbon Black Microparticle Surface in Aqueous Colloids Probed by Optical Second-Harmonic Generation†. *J. Phys. Chem. C* **2007**, *111*, 8708−8715.
(49) Doughty, B.; Rao, Y.; Kazer, S. W.; Kwok, S. J.; Turro, N. J.; Eisenthal, K. B. Probing the Relative Orientation of Molecules Bound to DNA through Controlled Interference Using Second-Harmonic Generation. *Proc. Natl. Acad. Sci. U. S. A.* **2013**, *110*, 5756−8.
(50) Rao, Y.; Kwok, S. J.; Lombardi, J.; Turro, N. J.; Eisenthal, K. B. Label-Free Probe of HIV-1 TAT Peptide Binding to Mimetic Membranes. *Proc. Natl. Acad. Sci. U. S. A.* **2014**, *111*, 12684−8.
(51) Wu, Y.; Li, W.; Xu, B.; Li, X.; Wang, H.; McNeill, V. F.; Rao, Y.; Dai, H. L. Observation of Organic Molecules at the Aerosol Surface. *J. Phys. Chem. Lett.* **2016**, *7*, 2294−2297.
(52) Qian, Y.; Deng, G. H.; Rao, Y. In Situ Chemical Analysis of the Gas-Aerosol Particle Interface. *Anal. Chem.* **2018**, *90*, 10967−10973.
(53) Cheng, Y.; Su, H.; Koop, T.; Mikhailov, E.; Poschl, U. Size Dependence of Phase Transitions in Aerosol Nanoparticles. *Nat. Commun.* **2015**, *6*, 5923.
(54) Tang, I. N.; Tridico, A. C.; Fung, K. H. Thermodynamic and Optical Properties of Sea Salt Aerosols. *J. Geophys. Res. [Atmos.]* **1997**, *102*, 23269−23275.
(55) Malijevsky, A.; Jackson, G. A Perspective on the Interfacial Properties of Nanoscopic Liquid Drops. *J. Phys.: Condens. Matter* **2012**, *24*, 464121.
(56) Altaf, M. B.; Freedman, M. A. Effect of Drying Rate on Aerosol Particle Morphology. *J. Phys. Chem. Lett.* **2017**, *8*, 3613−3618.
(57) Shen, Y. R.; Ostroverkhov, V. Sum-Frequency Vibrational Spectroscopy on Water Interfaces: Polar Orientation of Water Molecules at Interfaces. *Chem. Rev.* **2006**, *106*, 1140−54.
(58) Tian, C. S.; Shen, Y. R. Sum-Frequency Vibrational Spectroscopic Studies of Water/Vapor Interfaces. *Chem. Phys. Lett.* **2009**, *470*, 1−6.
(59) Tian, C. S.; Shen, Y. R. Structure and Charging of Hydrophobic Material/Water Interfaces Studied by Phase-Sensitive Sum-Frequency Vibrational Spectroscopy. *Proc. Natl. Acad. Sci. U. S. A.* **2009**, *106*, 15148−53.
(60) Eisenthal, K. B. Second Harmonic Spectroscopy of Aqueous Nano- and Microparticle Interfaces. *Chem. Rev.* **2006**, *106*, 1462−77.
(61) Feng, R. R.; Guo, Y.; Wang, H. F. Reorientation of the "Free OH" Group in the Top-Most Layer of Air/Water Interface of Sodium Fluoride Aqueous Solution Probed with Sum-Frequency Generation Vibrational Spectroscopy. *J. Chem. Phys.* **2014**, *141*, 18C507.
(62) Gan, W.; Wu, D.; Zhang, Z.; Guo, Y.; Wang, H.-f. Orientation and Motion of Water Molecules at Air/Water Interface. *Chin. J. Chem. Phys.* **2006**, *19*, 20−24.
(63) Buch, V.; Tarbuck, T.; Richmond, G. L.; Groenzin, H.; Li, I.; Shultz, M. J. Sum Frequency Generation Surface Spectra of Ice, Water, and Acid Solution Investigated by an Exciton Model. *J. Chem. Phys.* **2007**, *127*, 204710.
(64) Kido Soule, M. C.; Hore, D. K.; Jaramillo-Fellin, D. M.; Richmond, G. L. Differing Adsorption Behavior of Environmentally Important Cyanophenol Isomers at the Air-Water Interface. *J. Phys. Chem. B* **2006**, *110*, 16575−83.
(65) Gopalakrishnan, S.; Liu, D.; Allen, H. C.; Kuo, M.; Shultz, M. J. Vibrational Spectroscopic Studies of Aqueous Interfaces: Salts, Acids, Bases, and Nanodrops. *Chem. Rev.* **2006**, *106*, 1155−75.
(66) Rinuy, J.; Brevet, P. F.; Girault, H. H. Second Harmonic Generation of Glucose Oxidase at the Air/Water Interface. *Biophys. J.* **1999**, *77*, 3350−3355.
(67) Tamburello-Luca, A. A.; Hébert, P.; Antoine, R.; Brevet, P. F.; Girault, H. H. Optical Surface Second Harmonic Generation Study of

DOI: 10.1021/acs.jpca.9b03896
J. Phys. Chem. A 2019, 123, 6304−6312

the Two Acid/Base Equilibria of Eosin B at the Air/Water Interface. *Langmuir* **1997**, *13*, 4428−4434.
(68) Fedoseeva, M.; Fita, P.; Vauthey, E. Excited-State Dynamics of Charged Dyes at Alkane/Water Interfaces in the Presence of Salts and Ionic Surfactants. *Langmuir* **2013**, *29*, 14865−72.
(69) Moyano, F.; Silber, J. J.; Correa, N. M. On the Investigation of the Bilayer Functionalities of 1,2-Di-Oleoyl-Sn-Glycero-3-Phosphatidylcholine (DOPC) Large Unilamellar Vesicles Using Cationic Hemicyanines as Optical Probes: a Wavelength-Selective Fluorescence Approach. *J. Colloid Interface Sci.* **2008**, *317*, 332−45.
(70) Jee, A. Y.; Bae, E.; Lee, M. Internal Motion of an Electronically Excited Molecule in Viscoelastic Media. *J. Chem. Phys.* **2010**, *133*, 014507.
(71) Petrov, N. K.; Ivanov, D. A.; Kryukov, I. V.; Svirida, A. D.; Shandarov, Y. A.; Alfimov, M. V. The Time-Resolved Fluorescence Stokes Shift of Cucurbit[6]Uril Complexes with a Pyridinium Styryl Dye. *J. Fluoresc.* **2018**, *28*, 883−887.
(72) Eisenthal, K. B. Liquid Interfaces Probed by Second-Harmonic and Sum-Frequency Spectroscopy. *Chem. Rev.* **1996**, *96*, 1343−1360.
(73) Wang, H.; Troxler, T.; Yeh, A.-G.; Dai, H.-L. In Situ, Nonlinear Optical Probe of Surfactant Adsorption on the Surface of Microparticles in Colloids. *Langmuir* **2000**, *16*, 2475−2481.
(74) Nath, S. Surface Tension of Nonideal Binary Liquid Mixtures as a Function of Composition. *J. Colloid Interface Sci.* **1999**, *209*, 116−122.
(75) Nozière, B.; Baduel, C.; Jaffrezo, J. L. The dynamic surface tension of atmospheric aerosol surfactants reveals new aspects of cloud activation. *Nat. Commun.* **2014**, *5*. DOI: 10.1038/ncomms4335
(76) Petters, M. D.; Kreidenweis, S. M. A Single Parameter Representation of Hygroscopic Growth and Cloud Condensation Nucleus Activity. *Atmos. Chem. Phys.* **2007**, *7*, 1961−1971.
(77) Adamson, A. W. *Physical Chemistry of Surfaces*, 6th ed.; Wiley: New York,, 1997.
(78) Birdi, D. K. C. S. *Adsorption and the Gibbs Surface Excess*; Springer-Verlag: Boston, MA, USA, 1984.
(79) Craig, R. L.; Nandy, L.; Axson, J. L.; Dutcher, C. S.; Ault, A. P. Spectroscopic Determination of Aerosol pH from Acid-Base Equilibria in Inorganic, Organic, and Mixed Systems. *J. Phys. Chem. A* **2017**, *121*, 5690−5699.

DOI: 10.1021/acs.jpca.9b03896
J. Phys. Chem. A 2019, 123, 6304−6312